UNIVERSITY OF COPENHAGEN

Redox scanning in the study of metabolic zonation of liver.

Quistorff, Bjørn; Chance, Britton

Published in:
Regulation of Hepatic Metabolism

Publication date:
1986

Document version
Publisher's PDF, also known as Version of record

Citation for published version (APA):
Quistorff, B., & Chance, B. (1986). Redox scanning in the study of metabolic zonation of liver. *Regulation of Hepatic Metabolism*, 185-207.

Download date: 31. okt.. 2020

From: REGULATION OF HEPATIC METABOLISM
Edited by Ronald G. Thurman, Frederick C. Kauffman
and Kurk Jungermann
(Plenum Publishing Corporation, 1986)

Chapter 8

Redox Scanning in the Study of Metabolic Zonation of Liver

Bjørn Quistorff and Britton Chance

1. INTRODUCTION

The metabolic activity of an organ, e.g., the liver, will create gradients of oxygen, substrates, hormones, and products of metabolism along the capillaries. These concentration gradients will tend to subdivide the organ into zones of different metabolic activity at the capillary level. In many organs, e.g., muscles and brain, capillaries seem to be organized so as to minimize the zonation effect of the longitudinal capillary gradients, since adjacent parallel capillaries are perfused in opposite directions.

In the liver, however, microcirculation is organized, it seems, to obtain a maximum of zonation. Capillaries (sinusoids) in this organ form functional units in which adjacent sinusoids have adjacent exit points and flow in the same direction.[1] The response of the liver to various pathological conditions and toxic substances demonstrates clearly such a functional zonation of the parenchyma (for reviews, see Rappaport[1] and Jungermann and Katz[2]). At present, there is no clear understanding of the physiological significance of zonation.

The study of intercellular metabolic heterogeneity requires special tech-

BJØRN QUISTORFF • Department of Biochemistry, University of Copenhagen, 2200 Copenhagen, Denmark. BRITTON CHANCE • The Johnson Research Foundation, University of Pennsylvania, Philadelphia, Pennsylvania 19104.

niques, some of which are described in Chapters 3–7. Among other new and potentially useful techniques is a recently developed column technique, in which isolated hepatocytes are packed on a polyacrylamide column, effectively transforming the liver into one "macrosinusoid."[3] Further, a digitonin perfusion technique has been developed that allows specific release of intracellular material from periportal or perivenous cells.[4,4a] Finally, nuclear magnetic resonance (NMR) spectroscopy offers the possibility of noninvasive study of both inter- and intracellular compartmentation *in vivo*. Phosphorus NMR imaging has recently been achieved *in vivo*.[5] At present, however, the technique provides a resolution in the linear dimension of only 5–10 times the length of the sinusoid.

In this chapter, we describe the use of redox-ratio scanning in the study of metabolic zonation, employing a surface fluorescence technique, designed for three-dimensional (3-D) measurement on frozen tissue with a spatial resolution of approximately 2×10^{-7} ml.[6,7]

2. INDICATORS OF THE INTRACELLULAR REDOX STATE OF PYRIDINE NUCLEOTIDES

2.1. Indicator Metabolite Method

The term "intracellular redox state" is often used to indicate the redox state of one of the pyridine nucleotide redox couples, NAD^+/NADH and $NADP^+$/NADPH. According to Williamson *et al.*,[8] the redox state is defined as the ratio of the free concentrations of the reduced and oxidized pyridine nucleotide at thermodynamic equilibrium. The redox potential, E_h, is obtained by inserting this ratio into the Nernst equation employing the proper midpoint potential. Since the pyridine nucleotides are compartmentalized within the cells due to impermeability of most intracellular membranes to these molecules, the redox state must be specified for a specific intracellular compartment. In the context of this work, the relevant compartments are the mitochondrial and the cytosolic compartment. The most widely used method in assessing the redox state of the NAD^+/NADH or the $NADP^+$/NADPH redox couple is either the metabolite indicator method or direct spectrometric measurement of the fluorescence or absorption of the reduced species of the redox couple.

With the metabolite indicator method, a dehydrogenase reaction is chosen that is specific for either the mitochondrial or the cytosolic compartment and specific for the redox couple in question. Provided that thermodynamic equilibrium can be assumed in the dehydrogenase reaction, the redox ratio may be calculated from the equilibrium constant and the actual equilibrium concentrations of the substrates of the reaction. Table I shows examples of dehydrogenases that are commonly used in assessing the redox state of NAD^+/NADH and

Table I. Redox Indicator Metabolite Reactions and Redox Potentials in Liver[a]

Cytosolic space	Ref.	Mitochondrial space	Ref.
NAD/NADH −214 mV Lactate dehydrogenase	10	NAD/NADH −318 mV β-Hydroxybutyrate dehydrogenase	8, 12
NADP/NADPH −393 mV Isocitrate dehydrogenase 6-P-Gluconate dehydrogenase Malic enzyme	11, 12	NADP/NADPH −415 mV Isocitrate dehydrogenase Glutamate dehydrogenase	11, 13

[a] Modified from Sies.[11] The indicator metabolite systems are discussed in the references given in the table.

$NADP^+$/NADPH redox couples for the cytoplasmic and mitochondrial compartments in liver and other tisseus (for a recent review, see Sies[9]).

2.2. Tissue Fluorescence

Fluorescence measurement on intact tissue as a way of assessing the tissue redox state was first applied by Chance and Jöbsis[14] and Chance *et al.*[15] for reduced pyridine nucleotide (PN) and by Ramirez and Vega[16] for flavoprotein (FP). PN fluorescence from intact tissue is obtained as a broad peak at 450 nm after excitation with UV light, usually the mercury arc line at 366 nm. The signal originates predominantly from the pyridine nucleotides NADPH and NADH, which are present in the cell in both a free and a protein-bound form within the cytosolic and the mitochondrial compartment. In addition, however, there is a chemically undefined background fluorescence excited under the same conditions, some of which is related to lipids, but which does not seem to take part in metabolic redox transitions. This latter contribution to the PN fluorescence signal varies considerably among different tissues. The white matter of brain [17] and part of the epicardium[18] are examples of tissues with high PN fluorescence background. In the liver, this background fluorescence is comparatively small.[19]

The liver cell contains several FPs. Among these, however, the flavin moeity of the dehydrolipoamide dehydrogenase has by far the highest fluorescence yield.[20,21] This flavin is coupled to the mitochondrial NAD^+/NADH system by the pyruvate dehydrogenase and α-ketoglutarate dehydrogenase reactions.[22] More than 90% of the flavin signal originates from the mitochondrial compartment.[23]

Since fluorescence measurements on intact tissue require excitation light of high spectral purity and intensity, most work is done with fixed-wavelength instruments. Excitation–emission spectra obtained from isolated mitochondrial preparations are useful in assigning fixed wavelengths for PN and FP measurements. Figure 1 shows the excitation–emission spectra of oxidized and reduced

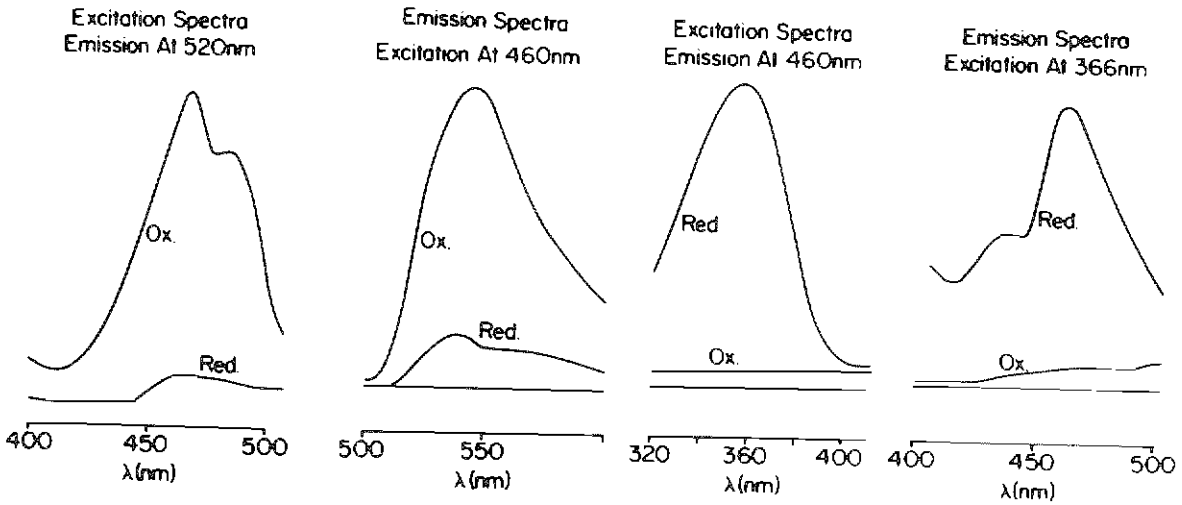

Figure 1. Low-temperature excitation–emission spectra for PN (366–460 nm) and FP (460–520 nm) for pigeon heart mitochondria. Reprinted from Chance *et al.*[24] with permission.

pigeon heart mitochondria at −196°C, the temperature at which the redox scanner operates. Compared with room temperature, there is a 7 to 14-fold (tissue-dependent) fluorescence enhancement of FP and PN signals with a much smaller enhancement of the background signal, thus improving the signal-to-noise ratio.[24] The PN fluorescence is attributed to NADH rather than NADPH, since cardiac mitochondria have little NADPH fluorescence.[25] The spectra of reduced mitochondria show high PN signal and very little FP signal and vice versa for oxidized mitochondria. FP may be excited between 405 and 500 nm usually with negligible excitation of PNs. Conversely, excitation of PN at 366 nm results in relatively little excitation of FP that is removed easily by appropriate secondary filters.

2.3. Different Pyridine Nucleotide Pools

2.3.1. Fluorescence Enhancement

In perfused organs, quantitative information on different PN pools may be obtained by simultaneous measurement of absorption (340 nm) and fluorescence, allowing calculation of the $\Delta F/\Delta A$ ratio, which may be taken as a measure of fluorescence quantum yield.[10,26] Since the fluorescence yield as well as the wavelength of maximum fluorescence and absorption depend on the chemical state of the reduced species of the PN redox couples, the $\Delta F/\Delta A$ ratio may be used to calibrate the response to different redox transitions. In the perfused rat liver, Bücher *et al.*[10] showed that the fluorescence yield changed 2.5-fold more with ethanol than with ammonium chloride. Further, the fluorescence yield of intracellular PN was 4 times larger than added, extracellular NADH.[10] Avi-Dor *et al.*[27] demonstrated in isolated rat liver mitochondria that the PN fluorescence yield was 4 times higher with β-hydroxybutyrate-induced redox changes than with ammonium chloride. The fluorescence enhancement of intracellular PN is due to specific binding to various dehydrogenases.[28] There are, however, exceptions: Binding to glyceraldehyde phosphate dehydrogenase in muscle decreases rather than increases the quantum efficiency of NADH fluorescence.[29]

2.3.2. Fluorescence Blue Shift

Another effect of NADH binding to protein is a shift toward the blue of the wavelength of maximum emission.[28] This blue shift of PN fluorescence is seen, however, only in isolated systems, e.g., isolated mitochondria,[30] not in intact organs.[31] Thorell and Chance[32] found large changes in the light-absorbing properties of isolated liver cells between 400 and 460 nm. It was therefore suggested[15] and later confirmed[31] that the difference between fluorescence emission peaks of isolated mitochondria and the corresponding intact tissues may be due to attenuation of the short-wavelength side of the fluorescence band by filter

effect of the tissue. However, even with suitable correction for this possible filtering effect, the fluorescence emission maximum varies in different types of tissues, probably as a result of quantitative or qualitative differences in binding sites.

2.3.3. Cytosolic vs. Mitochondrial Contribution to the Pyridine Nucleotide Fluorescence Signal

In skeletal and heart muscle, it is generally agreed that a majority of the PN fluorescence signal originates from the mitochondrial compartment.[33–35] In the brain, O'Connor *et al.*[36] found that PN fluorescence increases to a steady-state level after 30–40 sec of anoxia; however, chemically determined total NADH continues to increase along with an increase in the lactate concentration for the next 5 min to more than 2-fold the initial value obtained at the time steady-state fluorescence was obtained. O'Connor and co-workers thus concluded that the cytoplasmic NADH does not contribute significantly to PN fluorescence in brain. In the electric organ of the electric fish, however, the PN fluorescence signal is largely cytoplasmic, apparently due to the paucity of mitochondria in this organ.[37]

In the rat liver, the situation is somewhat different. From the studies of Scholz *et al.*,[23] it is apparent that PN fluorescence originates from both compartments. In the rotenone-inhibited perfused rat liver, pyruvate (2 mM) reversed about 50% of the PN fluorescence. Furthermore, in the anoxic perfused liver, pyruvate perfusion reversed about 40% of the PN fluorescence, but did not change the FP fluorescence. On the contrary, in the rotenone-inhibited liver, acetoacetate reversed the FP reduction almost completely, but reversed the PN reduction only partially. This experiment suggests that approximately half the PN fluorescence originates from the cytosol and half from the mitochondria, whereas the flavin fluorescence originates predominantly from the mitochondria. It was further observed that aminopyrine does not change the flavin fluorescence in the perfused liver, but causes an oxidation of PN in agreement with the aforestated conclusion.[23] This result also suggests that cytoplasmic flavin, e.g., flavin associated with the microsomal monooxygenation system, does not contribute significantly to the fluorescence signal.

2.4. Flavoprotein/Pyridine Nucleotide Ratio Method

We have used the ratio of the FP fluorescence signal to that of PN as a redox indication.[24] As shown in Fig. 1, only the oxidized species of the FP couple is fluorescent, and only the reduced species of the PN couple is fluorescent. With the reservations discussed above, the FP/PN ratio will reflect the redox state of the mitochondrial NAD/NADH redox couple. Since the two components of the redox ratio vary in opposite directions on a redox change, sensitivity will

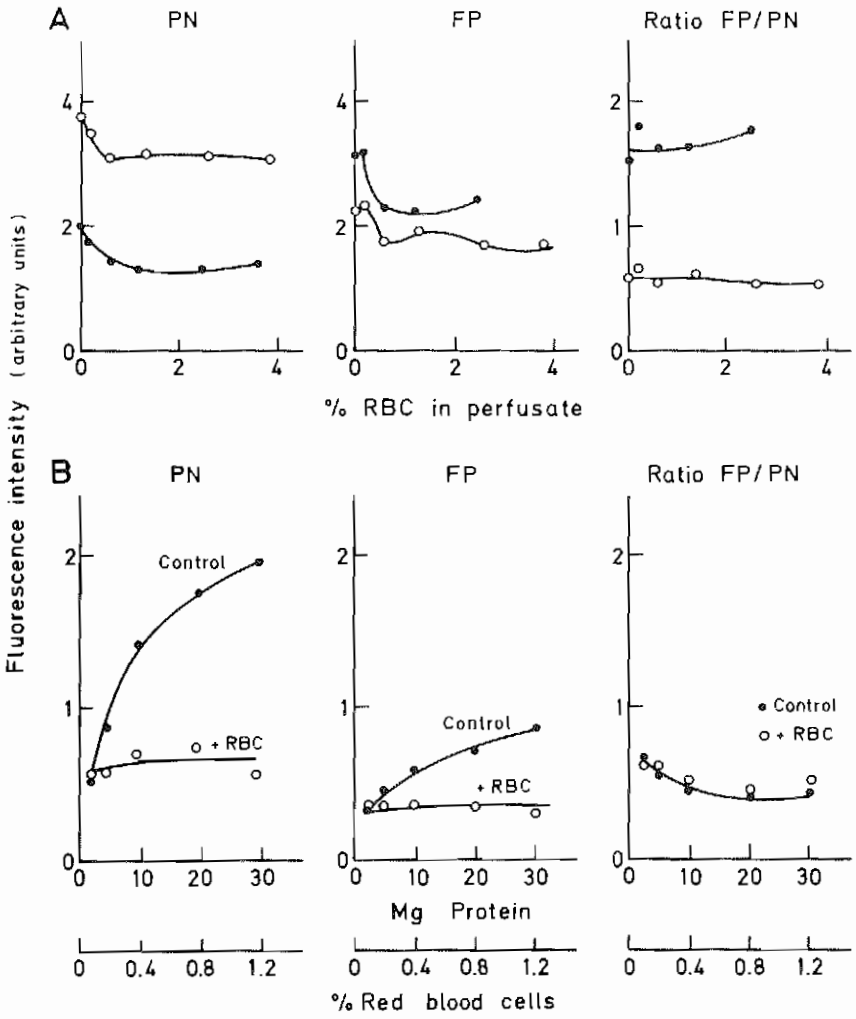

Figure 2. Effect of red blood cells (RBC) on PN and FP fluorescence. (A) PN, FP, and FP/PN signals were recorded by surface fluorometry on the perfused liver in the normoxic, ●, and the hypoxic state, ○. RBC volume was varied as indicated on the abscissa. (B) Isolated pigeon heart mitochondria and RBC were mixed in the concentrations given on the abscissa as mg mitochondrial protein and % RBC volume, respectively. The traces labeled *Control* are those obtained in the absence of RBC. Modified from Chance *et al.*[24]

be increased compared with recording of only one of the parameters. The FP PN ratio (called the calculated ratio) varies between 0.05 and 10 in isolated mitochondria,[24] while in intact tissue, the redox range is of the order of 2–4.[3,4]

In freeze trapping studies, the system should be stable at the trapped temperature for adequate time for precise measurement. While it might seem advantageous for redox state measurements to observe the cytochrome components of the frozen sample, particularly cytochrome oxidase, we have elected the FP/PN ratio.[24] One reason for this is that in the trapping procedure, oxygen, which is of crucial importance may not be readily trapped, and its diffusion in supercooled water may indeed greatly exceed expectations based upon freezing at 0°C.[40a] However, the FP/PN redox couple is well protected from perturbations of the cytochrome oxidase by diffusible oxygen by the 'freeze out' of electron transfer in the respiratory chain usually at the cytochrome *b* ubiquinone site. Thus, we have reasonable assurance that the freeze trapping of the FP/PN ratio affords fidelity of the room temperature redox state.

Another important quality of the redox ratio is its relative insensitivity to changes in mitochondrial concentration, interfering pigments, and red blood cells in the tissue. This is illustrated in Fig. 2A for a perfused rat liver in which the concentration of red blood cells (RBC) in the perfusate was varied. While FP and PN varied significantly with changes in blood concentration, the ratio was affected only slightly. Similarly, in Fig. 2B, the concentration of isolated mitochondria with or without RBC was varied. Again, the ratio was affected much less than the FP and PN signal alone. To interpret the observed changes in FP and PN fluorescence with respect to respiratory activity of the tissue being scanned, the concept of metabolic state of isolated mitochondria advanced by Chance and Williams[41] has proven very useful. Table II shows this relationship between the degree of reduction of PN and FP in five different metabolic states.

Table II. Metabolic State of Mitochondria and Associated Oxidation–Reduction Levels of Flavoprotein and Pyridine Nucleotide[a]

Characteristics of metabolic state						Steady-state reduction (%)	
State	O	ADP level	Substrate level	Respiration rate	Rate-limiting factor	FP	PN
1	>0	Low	Low	Slow	ADP	21	90
2	>0	High	0	Slow	Substrate	0	0
3	>0	High	High	Fast	Respiratory chain	20	53
4	>0	Low	High	Slow	ADP	40	99
5	0	High	High	0	Oxygen	100	100

[a]Data from Chance and Williams[41] (modified from Jöbsis and Lamanna[32]).

3. LOW-TEMPERATURE SCANNING TECHNIQUE

3.1. General Description

The scanning instrument is shown in Fig. 3. The technique is based on automated scanning of fluorescence signals from the surface of frozen tissue with a micro-light guide. The parameters measured are the pyridine nucleotide (PN) and flavoprotein (FP) fluorescence signals as discussed above.

The frozen liver sample, which may be obtained by a number of different freeze–quenching techniques, is mechanically fixed in the Dewar flask of the instrument filled with liquid nitrogen, as shown in Fig. 4. Redox-ratio scanning is performed as follows: A flat surface on the sample is created by milling the sample at 77°K.[42] The micro-light guide is then placed over an appropriate point on the tissue sample and moved across the surface under computer control, while the optical signals from each point are read and stored by the computer. The instrument now allows for another scan of the same sample at a deeper level. This is carried out by milling away the surface of the specimen to any desired depth and repeating the scan as described. In this way, a series of consecutive scans from the same sample may be collected. The scans will be identical in size and shape and will be aligned vertically. Such a data set may thus be used for a 2- and/or 3-D reconstruction of a "metabolic representation" of the sample in terms of redox state.

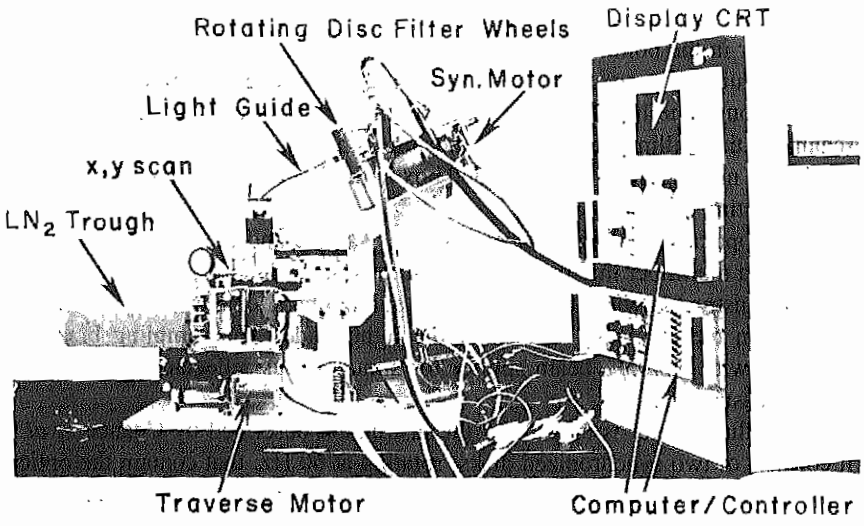

Figure 3. Redox-ratio scanning instrument. See the text for details.

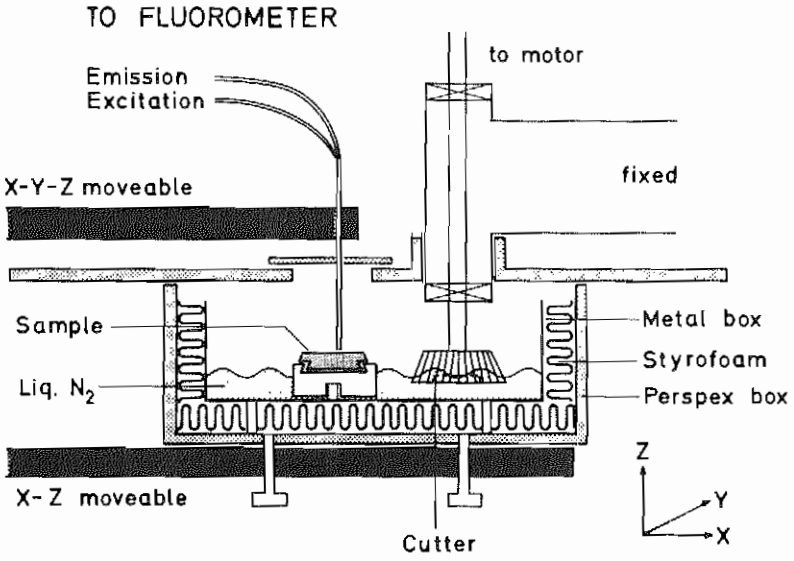

Figure 4. Simplified diagram of the redox-ratio scanning instrument. Fluorescence signals are measured from the frozen sample by moving the micro-light guide across the surface, point by point. FP and PN are recorded from each point. When a scan is completed, 50–100 μm is milled off the sample and the scan is repeated on the new surface. Reprinted from Quistorff and Chance[42] with permission.

3.2. Details of the Instrument

The instrument is shown schematically in Fig. 4. The sample is mounted in a holder in the bottom of a Styrofoam-insulated metal box, containing about 250 ml liquid nitrogen. A milling head suited for low-temperature milling protrudes through the lid of the box for grinding the surface of the tissue. During scanning, the milling head is in liquid nitrogen. Milling of the surface is performed by moving the whole insulated box in the X and Z directions with respect to the rotating milling head.[42]

The optical coupling between the liver sample and the fluorometer is obtained by a multifiber micro-light guide of the one-end-fused two-branch type,[43] usually constructed with 50-μm-diameter quartz fibers. The mercury arc light is focused on the excitation branch of the light guide. The sampling branch is equipped with a 5/95% beam splitter for simultaneous reflectance and fluorescence measurements.

The fluorometer is essentially the instrument described by Chance *et al.*[44] It consists of two synchronized disks, rotating at 60 Hz, that contain the optical filters. Each disk has four positions for filters. For redox-ratio measurements, two channels are used: for PN and FP. The reflectance signals obtained at the FP and PN excitation wavelengths may be recorded simultaneously in the two

other channels. For PN, the excitation wavelength 366 nm is used; for PN emission, a filter combination is employed giving peak transmission at 450 nm. For FP, the corresponding values for excitation and emission are 436 and 520 nm, respectively.[7]

After integration and analog-to-digital conversion, the fluorescence signals are read and stored by a computer. The data may be presented in a variety of ways, e.g., as television images of single scans (see Figs. 9 and 10), in which a scan is composed of a number of pixels corresponding to the number of points scanned on the particular tissue surface. As a standard procedure, we use a gray scale for the display of the redox images in which black represents a low number (reduced) and white represents a high number (oxidized).[7]

4. SPATIAL RESOLUTION OF THE INSTRUMENT

The 2-D resolution in the scanning plane is strictly a function of light-guide size and geometry and of the distance between the tissue surface and the light guide. This relationship has been dealt with elsewhere.[43] With a fiber diameter of 50 μm and a tissue–light guide distance of 30–50 μm, which have been used in the experiments reported herein, the area covered is approximately 0.004 mm^2. The resolution down through the tissue is somewhat more complex, being determined by a number of different factors such as the absorption of both the excitation light and the emitted fluorescence by the tissue. In addition, this internal filtering effect may be wavelength-specific, especially for the excitation light.[31] The fact that readings in vertically aligned 2-D scans separated by only 50 μm may change by more than 100% suggests that the actual reading depth may be even less than 50 μm. However, assuming 50 μm as the depth of reading, the 3-D resolution of the instrument may be calculated to 2×10^{-7} ml, corresponding to 20–30 hepatocytes.

5. FREEZE–QUENCHING OF TISSUE

The tissue scanner is designed to analyze the 2- or 3-D distribution of metabolic states in freeze–trapped tissues. Freeze trapping has several significant advantages for this type of study in the liver: It quenches (1) metabolic processes, giving a "snapshot" of the metabolic state of the tissue. (2) It fixes the sample mechanically to a holder, which allows mounting in the instrument (see Fig. 6A and B). (3) It allows an investigation of the distribution of the metabolic states in three dimensions throughout the sample. (4) The fluorescence quantum yield of the flavoprotein and especially of the pyridine nucleotide is increased severalfold due to the low temperature, thus improving the signal-to-noise ratio.[32]

We have used various freezing methods, each of which was selected to suit

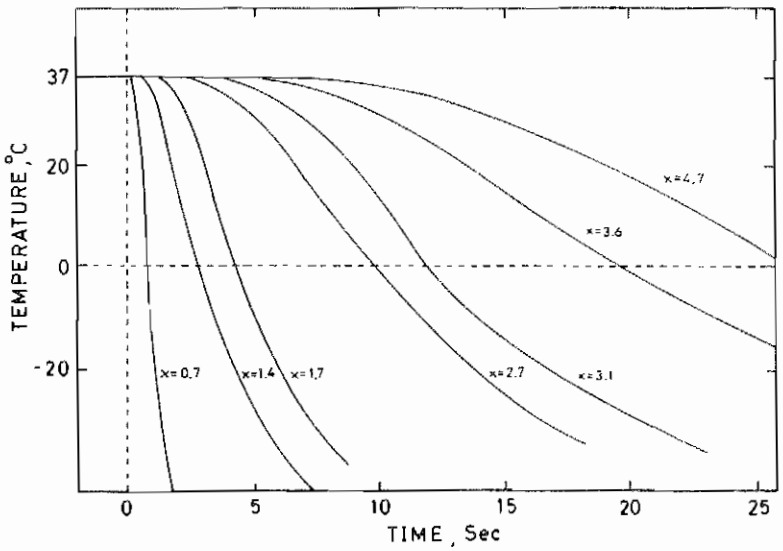

Figure 5. Time–course of freezing at different distances from the cooled surface in a freeze–clamped rat brain. Temperature was recorded with a thermocouple inserted at various positions in the brain prior to freeze–clamping. (×) equals depth in mm from surface to center of thermocouple. Reprinted from Quistorff.[45]

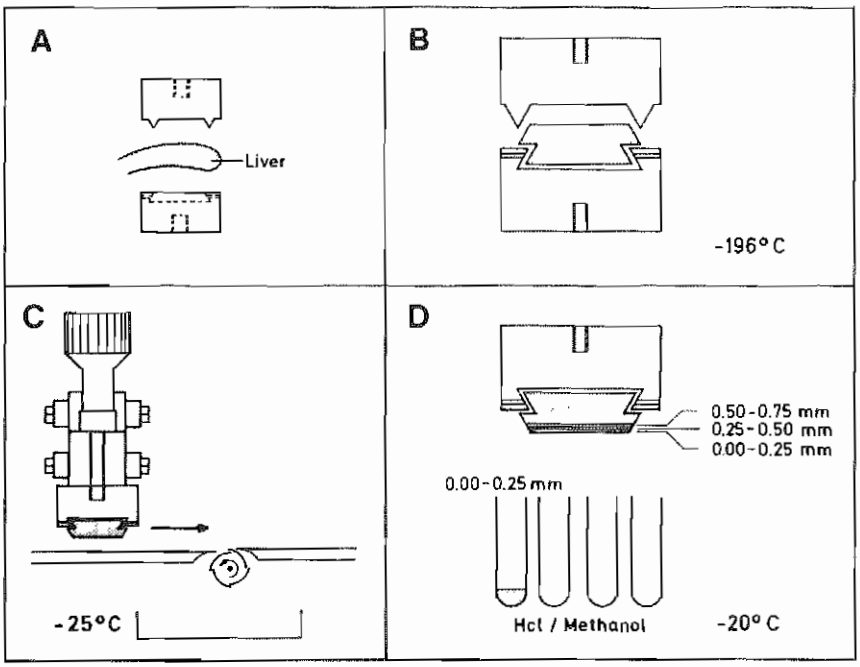

Figure 6. Steps in the procedure for freeze–clamping of rat liver and analysis of metabolites along the freezing gradient.

the particular tissue and experimental goal. If the aim of the particular experiment is to obtain measurements that reflect the *in vivo* state, the freeze-quenching procedure must be designed accordingly, i.e., to obtain the shortest possible time interval between interruption of normal circulation and quenching of metabolic processes.[45] Even under optimal conditions, this implies that only small tissue samples or thin wafers of tissue can be used, since the freezing time in the tissue increases exponentially with distance from the cooled surface, as demonstrated in Fig. 5.

For 3-D studies with the redox scanning technique, it is therefore important to know the exact manner in which each tissue is frozen and to check which part of the sample still reflects the *in vivo* state.[42,45] This may be controlled by chemical analysis of the [ATP/(ADP × P_i)] ratio along the freezing gradient of the freeze–clamped liver as by means of the technique illustrated in Fig 6. Applying this technique, Quistorff and Poulsen[46] found that freeze–clamped liver samples preserved the metabolic state to a depth of about 1 mm.

6. EXAMPLES OF SCANNING RESULTS

6.1. Histogram Distribution of Redox States

The size of the microcirculatory unit of the liver is of the order of 0.5 mm in diameter.[1] To include a reasonable number of such units, scans of liver usually cover an area of 4–16 mm^2. With 50 μm per light-guide step, this corresponds to 1600–6400 single-point readings of flavoprotein (FP) and pyridine nucleotide (PN) fluorescence. If carried out as a serial section scan to a depth of 1 mm, the total number of data points for such a 3-D scan at 50-μm resolution amounts to 32,000–128,000. Figure 7 shows the frequency distribution of the FP/PN ratio from a 13-section scan of a control liver at a resolution of 50 μm. On the x axis, the redox ratio is displayed, while the y axis shows the number of points in the scan in which a particular FP/PN value was recorded. On the z axis, the scanning depth below the sample surface is indicated.

Since the individual 2-D scans cover cross sections of 50–60 presumably functionally identical microcirculatory units at different cross-sectional levels, the redox-ratio distribution of a single 2-D scan may be regarded as a measure of the average redox-ratio distribution of the microcirculatory unit. On the basis of knowledge of the structure of the liver, one would not expect this average redox distribution to change with distance from the surface, except, perhaps, for the first 50–100 μm. Figure 8 confirms this assumption. Furthermore, the fact that no reduction of the average redox ratio is observed with increased distance from the surface suggests that the freeze–clamping of the sample was sufficiently fast to ensure quenching of all parts of the tissue block before the onset of anoxia.

A number of different redox perturbations have been tried on the perfused

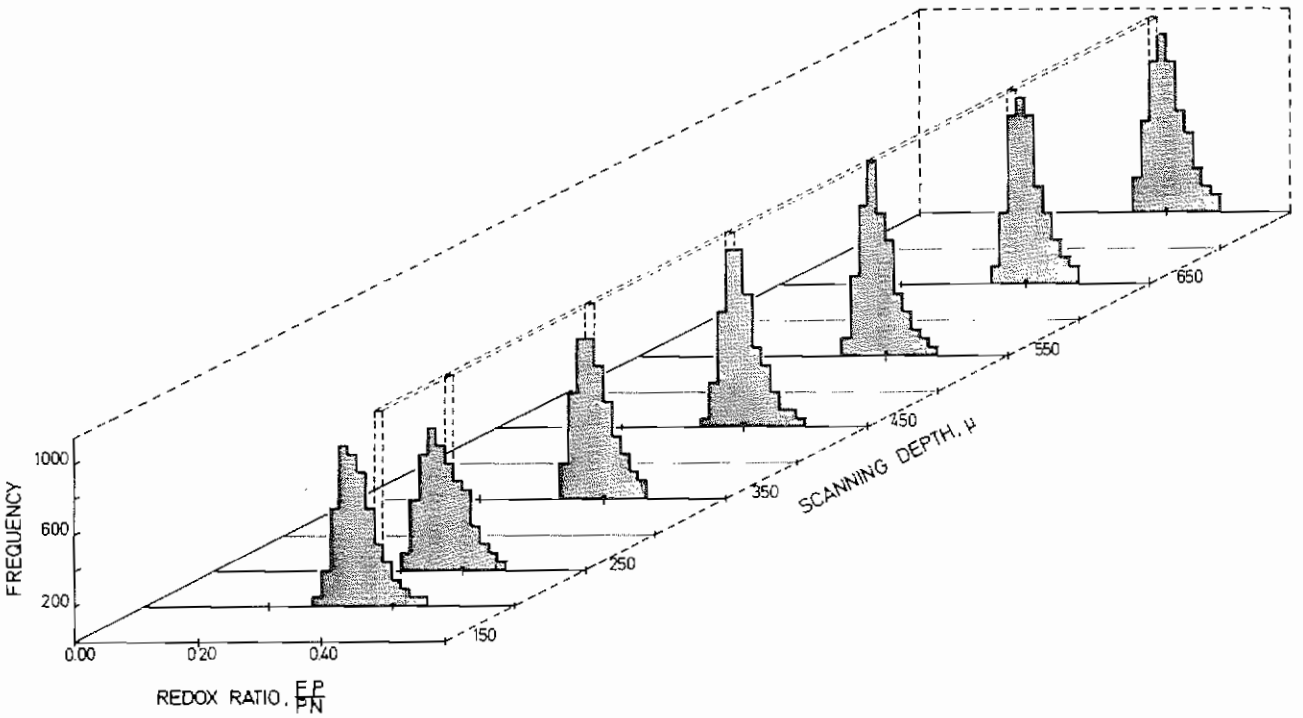

Figure 7. Frequency-distribution histogram of the FP/PN ratio for 13 consecutive scans of a freeze-clamped perfused rat liver. Prior to freezing, the liver was perfused for 20 min with Krebs–Henseleit–bicarbonate buffer, equilibriated with O_2 : Co_2 95 : 5 (vol. %). Each histogram represents one scan of 3.5 × 3.5 mm with 5041 single-point measurements of the FP/PN ratio. Only every second histogram is displayed for reasons of clarity. Reprinted from Quistorff and Chance.[39]

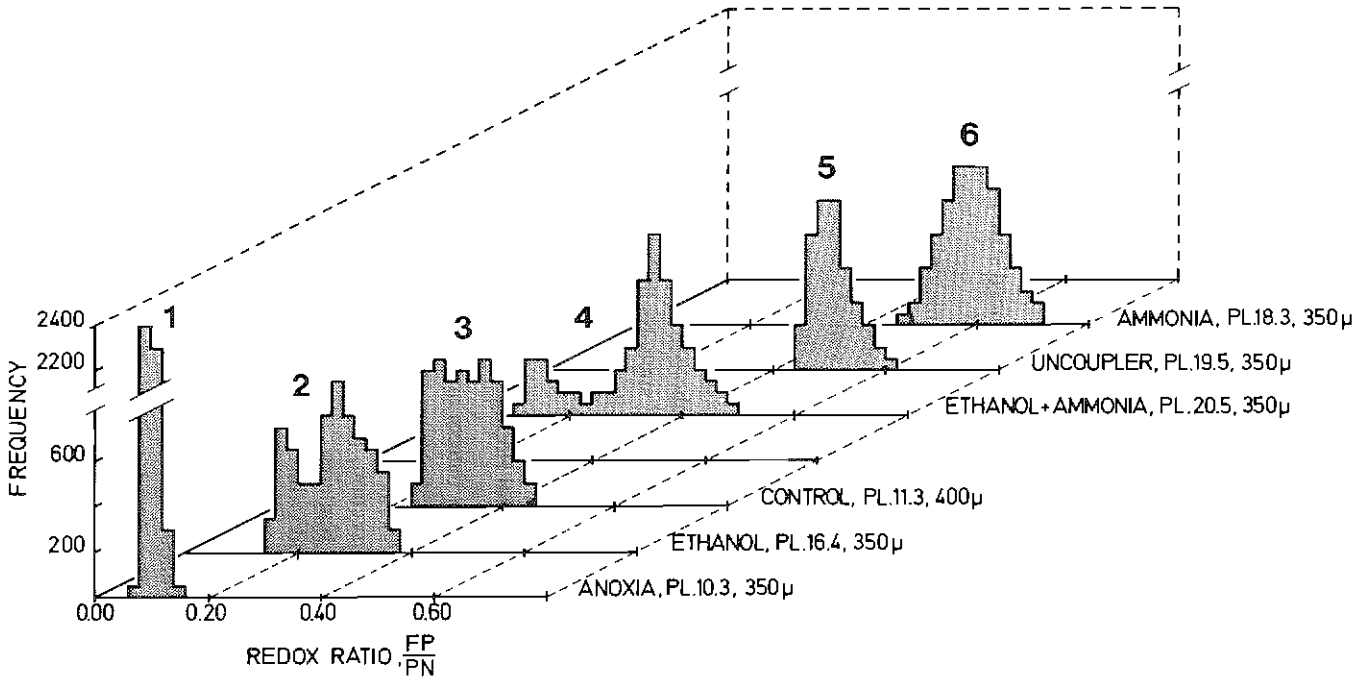

Figure 8. Frequency-distribution histograms of the FP/PN ratio. Shown are typical histograms from a number of different experiments with different redox perturbations. (1) The anoxic liver was freeze–clamped after having been left unperfused for 10 min (5 min at room temperature followed by 5 min on ice) and was covered with oxygen-impermeable foil. (2) Ethanol (6 mM) was included in the perfusate for 15 min prior to freeze–clamping. (3) Scan from control liver. (4) Ethanol (6 mM) and ammonium chloride (1 mM) were included in the perfusate 4 × 4 mm scan with 6561 data points at a resolution of 50 μm (5) Uncoupler [carbonylcyanide-*m*-chlorophenylhydrazone (CCCP)] (0.02 mM) was included in the perfusate for 15 min prior to freeze–clamping. (6) Ammonium chloride (1 mM) was included in the perfusate. All histograms, except histogram 4, represent 6 × 6 mm scans at a resolution of 100 μm, with 3721 data points per scan.

liver. Figure 8 shows examples of such experiments, presented as typical frequency-distribution histograms of the FP/PN ratio. Histogram 1, from an anoxic liver, shows a maximally reduced state and very narrow redox-ratio range. In fact, the 2-D redox ratio image of the anoxic liver (not shown) is completely without pattern. This allows the very important conclusion that liver morphology *per se* does not contribute any pattern to the redox scan.

With ethanol in the perfusate (histogram 2), the average redox ratio decreases to approximately 60% of control, in agreement with the well-known effect of ethanol on both the lactate/pyruvate and the hydroxybutyrate/acetoacetate ratio.[47] However, the histogram appears to have aquired a bimodal shape. One population of hepatocytes (25%) is highly reduced, while the majority of the readings reflect a somewhat reduced state but still within the control range.[48]

As would be expected, both uncoupler and ammonium chloride cause an increase of the average redox ratio, the increase being approximately 2-fold for ammonia (histogram 6) and 1.6-fold for uncoupler (histogram 5). Interestingly, the oxidation caused by ammonia seems to be almost completely eliminated by simultaneous addition of ammonia and ethanol (histogram 4). With this perturbation, about 25% of the readings become highly reduced, comparable to the reduced fraction of the ethanol histogram, while the remaining part is within the control range. An explanation of this result must await further experiments, but it is possible that zonation of either the metabolism of ammonia or that of ethanol plays a role. Recent work by Häussinger[49] supports the concept of zonation of the metabolism of ammonia. On the other hand, Kashiwagi *et al.*[50] do not find a zonation of the metabolism of ethanol.

6.2. Two- and Three-Dimensional Redox-Ratio Images

Figure 9 shows the 2-D redox pattern of a control liver *in vivo*. The FP/PN ratio is displayed on a gray scale covering the interval 0.48–0.22, with white as oxidized and black as reduced. The observed pattern represents a "redox image" of the particular liver section, rather than a structural image. The scan may be described as regularly scattered "reduced dots" (black) on a more or less uniformly oxidized background (white), very much resembling the well-known and characteristic lobular morphology of the liver. The reduced dots are 0.3–0.5 mm in diameter with a center-to-center distance of about 0.8 mm. We interpret the pattern as the white areas being the oxidized periportal space and the reduced black spots being the perivenous area. We have encircled what could be a classic lobule in Fig. 9, including a reduced perivenous area in the middle, surrounded by a number of "metabolic acini."[1]

On the basis of perfusion with india ink, Ji *et al.*[51] suggested that the darker spots on the surface of the hemoglobin-free perfused liver corresponded to the perivenous area in the rat liver. When FP/PN scans were compared with reflec-

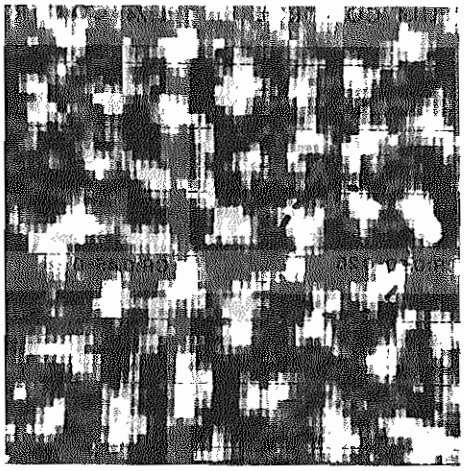

Figure 9. Television display of FP/PN scan from a control rat liver *in vivo*. The liver was freeze–clamped *in situ* as described in Quistorff and Chance.[42] The image represents a 6 × 6 mm area at a resolution of 100 μm and a depth of 400 μm, and was reconstructed from 3721 single-point measurements of the FP and PN fluorescence.

tance scans of the same surface, the lighter areas (more reflectance) of the latter corresponded to the oxidized parts of the FP/PN scans, thus supporting the aforedescribed interpretation of the redox pattern. However, the final proof will of course be an experiment in which a histological examination of the scanned surface confirms oxidized area as periportal space.

Figure 10 shows scans from freeze–clamped perfused livers. Two controls, one scanned at a resolution of 100 μm (left column) and another scanned at a resolution of 50 μm (middle column) are shown. The right-hand column shows a scan of a liver in which ethanol (6 mM) was included in the perfusate. For all three scans, the PN, the FP, and the calculated FP/PN ratio image are given. Note that different gray scales are used for the different images. In all images, however, a high number is represented in white and a low number in black. Compared with the *in vivo* scan in Fig. 9, the perfused control liver (Fig. 10, left column) shows an almost identical pattern. It is noteworthy that the FP and images actually show inverse patterns, except in a few localized spots where the signal is very low in both channels. The effect of ethanol on the 2-D redox pattern (Fig. 10, right column) is a significant increase in the reduced perivenous area and a much steeper transition between the periportal and perivenous areas. In most locations, the transition occurs within the linear resolution of the scan, i.e., 50 μm. On examination of the 2-D FP/PN scans of Fig. 10, one may recognize, in the outline of the reduced perivenous area in both the ethanol and the control liver, the so-called "starfish" shape found histologically in the liver in various pathological conditions,[1] supporting the concept of metabolic zonation.[2]

One of the virtues of the redox-ratio scanning technique is the ability to obtain information on 3-D metabolic structure. Figure 11 shows examples of

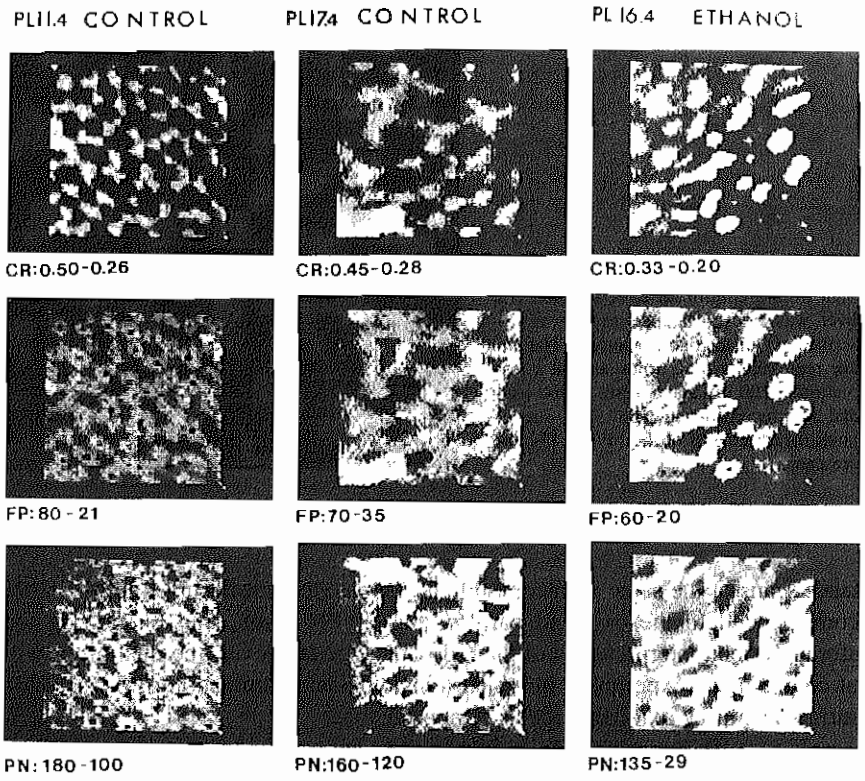

Figure 10. Television display of FP, PN, and FP/PN scans from perfused rat liver. The liver was perfused as described in the Fig 7 caption. The control liver (PL11.4) represents a 6 × 6 mm scan with 3721 data points at 100-μm resolution. The other control (PL17.4) represents a 3.5 × 3.5 mm scan with 5041 data points recorded at a resolution of 50 μm. The scan in the right-hand column is from a liver for which ethanol (6 mM) was included in the perfusate for 15 min prior to freeze-clamping. Scan size and resolution were as for control PL17.4. In all scans, the gray scale used represents a high number as white and a low number as black.

this for perfused rat liver. Figure 11A is from a control and Fig. 11B from an ethanol-perfused liver. It is obvious from the 2-D scans in Figs. 9 and 10 that there is a relatively well defined border zone in the FP/PN image. It was therefore convenient to reconstruct the 3-D data from the liver with only two gray levels, white as oxidized and black as reduced. The tissue block represented in the control (Fig. 11 A) was 2.9 × 2.9 × 0.9 mm, reconstructed from 5400 singlepoint measurements of the FP/PN ratio. For the ethanol-perfused liver (Fig. 11B), the tissue block was 1.9 × 1.9 × 0.55 mm, reconstructed from 16,000 points. Both models clearly show that the 2-D pattern of the consecutive scans forms a consistent 3-D structure, which may be interpreted as above in terms of the oxidized zones (white) and the reduced zones (black) being periportal and

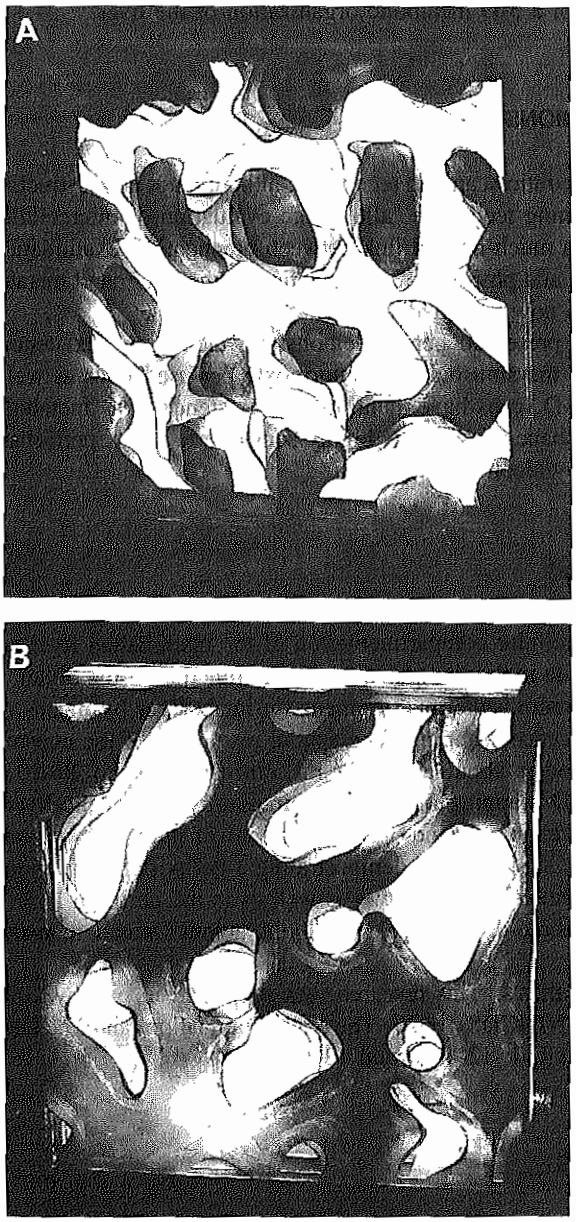

Figure 11. Three-dimensional redox-ratio model of perfused liver. (A) Control liver; (B) ethanol (6 mM)-perfused liver. Both models are seen from the surface of the liver. Modified from Quistorff and Chance.[39]

perivenous spaces, respectively. These figures demonstrated for the first time the existence of a 3-D metabolic organization of the liver.[48]

7. CONCLUSIONS

The redox-ratio scanning technique, although not nondestructive when used as a 3-D scanning technique, allows the evaluation of intercellular redox gradients. Thus, a much-needed link between biochemical examination of average organ function and physiological evaluation of the integrated metabolic function of the organ is now provided.

The data presented herein demonstrate clearly the existence of a redox gradient along the sinusoid of the normoxic perfused liver as well as for liver *in vivo*. The 3-D scans have identified the existence of a "metabolic acinus" in the liver, the shape of which is highly sensitive to redox perturbations such as those caused by alcohol metabolism.

8. SUMMARY

The intercellular compartmentation of the mammalian liver seems to play an important role in the integrated metabolic function of the organ. This chapter has discussed redox-state measurements in intact liver by means of automated surface fluorescence scanning. The spatial resolution of the current redox-ratio scanning method is about 2×10^{-7} ml, corresponding to 20–30 hepatocytes. This allows 3-D mapping of the microcirculatory unit of the liver in terms of redox state. Available 2- and 3-D redox scans of liver with various redox perturbations were summarized, demonstrating a periportal–perivenous redox gradient in the normoxic liver *in vivo* as well as in the perfused liver. Finally, the existence of a three-dimensional "metabolic acinus" was demonstrated.

ACKNOWLEDGMENTS. This research was supported in part by Grants USPHS-AA-05662 and NINCDS-10939, The Novo Foundation, and The Danish Medical Research Council, J. 12-4549 and 12-5473.

REFERENCES

1. Rappaport, A. M., 1980, Hepatic blood flow: Morphologic aspects and physiologic regulation, in: *Liver and Biliary Tract Physiology I*, Vol. 21 (N. B. Javitt, ed.), pp. 1–63, *Int. Rev. Physiol.*, University Park Press, Baltimore.
2. Jungermann, K., and Katz, N., 1982, Functional hepatocellular heterogeneity, *Hepatology* **2**(3):385–395.

3. Quistorff, B., 1983. The use of a hepatocyte column in the study of metabolic zonation in the liver, in: *Isolation, Characterization, and Use of Hepatocytes* (R. A. Harris and N. W. Cornell, eds.), pp. 131–137, Elsevier, New York.
4. Quistorff, B., Grunnet, N., and Cornell, N. W., 1985, Digitonin perfusion of rat liver: A new approach in the study of intraacinar and intracellular compartmentation in the liver, *Biochem. J.* **226**: 289–297.
4a. Quistorff, B., 1985. Gluconeogenesis in periportal and perivenous hepatocytes of rat liver, isolated by a new high-yield, digitonin–collagenase perfusion technique, *Biochem. J.* **229**:221–226.
5. Haselgrove, J. C., Subramanian, V. H., Leigh, J. S., Jr., Gyulai, L., and Chance, B., 1983, *In vivo* one-dimensional imaging of phosphorus metabolites by phosphorus-31 nuclear magnetic resonance, *Science* **220**:1170–1173.
6. Quistorff, B., and Chance, B., 1977, Two- and three dimensional analysis on brain oxygen delivery, in: *Oxygen and Physiological Function* (F. F. Jöbsis, ed.), pp. 100–110, Professional Information Library, Dallas.
7. Quistorff, B., Haselgrove, J. C., and Chance, B., 1985, High spatial resolution read-out of 3-D metabolic organ structure: An automated, low-temperature redox ratio scanning instrument, *Anal. Biochem.* **148**:389–400.
8. Williamson, D. H., Lund, P., and Krebs, H. A. 1967, The redox state of free nicotinamide-adenine dinucleotide in the cytoplasm and mitochondria of rat liver, *Biochem. J.* **103**:514–527.
9. Sies, H., 1982, Nicotinamide nucleotide compartmentation, in: *Metabolic Compartmentation* (H. Sies, ed.), pp. 205–231, Academic Press, London.
10. Bücher, T., Brauser, B., Conze, A., Klein, F., Langguth, O., and Sies, H., 1972. State of oxidation–reduction and state of binding in cytosolic NADH-systems as disclosed by equilibration with extracellular lactate/pyruvate in hemoglobin-free perfused rat liver, *Eur. J. Biochem.* **27**:301–317.
11. Sies, H., 1977, Redox compartmentation: A survey with emphasis on current problems, in: *Alcohol and Aldehyde Metabolizing Systems*, Vol. 3 (R. G. Thurman, J. R. Williamson, H. Drott, and B. Chance, eds.), pp. 47–64, Academic Press, New York.
12. Krebs, H. A., 1966, The redox state of NAD in the cytoplasm and mitochondria of rat liver, *Adv. Enzyme. Regul.* **5**:409–437.
13. Hoek, J. B., and Ernster, L., 1974, Mitochondrial transhydrogenase and the regulation of cytosolic reducing power, in: *Alcohol and Aldehyde Metabolizing Systems*, Vol. 1 (R. G. Thurman, Y. Yonetani, J. R. Williamson, and B. Chance, eds.), pp. 351–364, Academic Press, London.
14. Chance, B., and Jöbsis, F. F., 1959, Changes in fluorescence in a frog sartorius muscle following a twitch, *Nature (London)* **4681**:195–197.
15. Chance, B., Cohen, P., Jöbsis, F. F., and Schoener, B., 1962, Intracellular oxidation–reduction states *in vivo*, *Science* **137**:449–508.
16. Ramirez, J., and Vega, J., 1965, Cambios de la fluorescencia del musculo cardiaco durante la actividad mecanica, *Acta Physiol. Lat. Am.* **15**:239–240.
17. Welsh, F. A., O'Connor, M. J., and Langfitt, T. W., 1977, Regions of cerebral ischemia located by pyridine nucleotide fluorescence, *Science* **198**:951–953.
18. Barlow, C. H., and Chance, B., 1967, Ischemic areas in perfused rat hearts: Measurement by NADH fluorescence photography, *Science* **193**:909–910.
19. Chance, B., Schoener, B., Krejci, K., Rüssmann, W., Wessmann, W., Schnitger, H., and Bücher, T., 1965, Kinetics of fluorescence and metabolite changes in rat liver during a cycle of ischaemia, *Biochem. Z.* **341**:325–333.
20. Chance, B., and Schoener, B., 1966, Fluorometric studies of flavin component of the respiratory chain, in: *Flavins and Flavoproteins* (E. C. Slater, ed.), pp. 510–519, Elsevier, Amsterdam.
21. Hassinen, I., and Chance, B., 1968, Oxidation–reduction properties of the mitochondrial flavoprotein chain, *Biochem. Biophys. Res. Commun.* **31**(6):895–900.

22. Chance, B., Mela, L., and Wong, D., 1968. Flavoproteins of the respiratory chain, in *Flavins and Flavoproteins*, (K. Yagi, ed.), pp. 107–121, University Park Press, Baltimore
23. Scholz, R., Thurman, R. G., Williamson, J. R., Chance, B., and Bücher, T., 1969. Flavin and pyridine nucleotide oxydation–reduction changes in perfused rat liver: Anoxia and subcellular localization of fluorescent flavoproteins, *J. Biol. Chem.* **244**(9):2317–2324.
24. Chance, B., Schoener, B., Oshino, R., Itshak, F., and Nakase, Y., 1979. Oxidation–reduction ratio studies of mitochondria in freeze-trapped samples, *J. Biol. Chem.* **254**:4764–4771.
25. Chance, B., Williamson, J. R., Jamieson, D., and Schoener, B., 1965. Properties and kinetics of reduced pyridine nucleotide fluorescence of the isolated *in vivo* rat heart, *Biochem. Z.* **341**:357–377.
26. Sies, H., Häussinger, D., and Grosskopf, M., 1974. Mitochondrial nicotinamide nucleotide systems: Ammonium chloride responses in hemoglobin-free perfused liver, *Hoppe-Seyler's Z. Physiol. Chem.* **355**:305–320.
27. Avi-Dor, Y., Olson, J. M., Doherty, M. D., and Kaplan, N. O., 1962. Fluorescence of pyridine nucleotides in mitochondria, *J. Biol. Chem.* **237**(7):2377–2383.
28. Boyer, P. D., and Theorell, H., 1956. The changes in reduced NAD (NADH) fluorescence upon combination with liver ADH, *Acta Chem. Scand.* **10**:447–450.
29. Velick, S. F., 1958. Fluorescence spectra and polarization of glyceraldehyde-3-P- and lactic dehydrogenase coenzyme complexes, *J. Biol. Chem.* **233**(6):1455–1467.
30. Chance, B., and Baltscheffsky, H., 1958. Respiratory enzymes in oxidative phosphorylation. VII. Binding of intramitochondrial reduced NAD(P), *J. Biol. Chem.* **233**(3):736–739.
31. Galeotti, T., Rossum, D. V. van, Mayer, D. H., and Chance, B., 1970. On the fluorescence of NAD(P)H in whole cell preparation of tumours and normal tissues, *Eur. J. Biochem.* **17**:485–496.
32. Thorell, B., and Chance, B., 1960. Microspectrography of respiratory enzymes within the single cell under different metabolic conditions, *Exp. Cell Res.* **20**:43–55.
33. Jöbsis, F. F., and Duffield, J. C., 1967. Oxidative and glycolytic recovery metabolism in muscle, *J. Gen. Physiol.* **50**:10109–1047.
34. Chapman, J. B., 1972. Fluorometric studies of oxidative metabolism in isolated papillary muscle of the rabbit, *J. Gen. Physiol.* **59**:135–154.
35. Williamson, J. R., 1965. Glycolytic control mechanisms, *J. Biol. Chem.* **240**:2308–2318.
36. O'Connor, M. J., Welsh, F., Komarnicky, L., Davis, T., Stevens, J., Lewis, D., and Herman, C., 1977. Origin of labile NADH tissue fluorescence, in: *Oxygen and Physiological Function* (F. F. Jöbsis, ed.), pp. 90–99, Professional Information Library, Dallas.
37. Anbert, X., Chance, B., and Keynes, R. D., 1964. Optical studies of biochemical events in the electric organ of *Electrophorus*, *Proc. R. Soc. London Ser. B.* **160**:211–233.
38. Haselgrove, J. C., Barlow, C. H., and Chance, B., 1980. The 3-D distribution of metabolic states in the gerbil brain during the course of spreading depression, in: *Cerebral Metabolism and Neuronal Function* (J. V. Passonneau, R. A. Hawkins, W. D. Lust, and F. A. Welsh, eds.), pp. 72–76, Williams & Wilkins, Baltimore.
39. Quistorff, B., and Chance, B., 1982, 3-Dimensional recording of metabolic structure of rat liver: Evidence for a dynamic spatial ordering of liver metabolism, in: *Alcohol and Alcohol Metabolism: First Symposium on Alcohol* (J. Wadstein, ed.), pp. 21–39, Ferrosan, Malmö, Sweden.
40. Chance, B., and Quistorff, B., 1978. Study of tissue oxygen gradients by single and multiple indicators, in: *Oxygen Transport to Tissue—III* (I. A. Silver, M. Erecińska, and H. I. Bicher, eds.), pp. 331–338, Plenum Press, New York.
40a. Erecińska, M., and Chance, B., 1972. Studies on the electron transport chain at subzero temperatures: Electron transport at site III, *Arch. Biochem. Biophys.* **151**:304–315.
41. Chance, B., and Williams, G. R., 1957, The respiratory chain and oxidative phosphorylation, *Methods Enzymol.* **17**:65–134.

42. Quistorff, B., and Chance, B., 1980, Simple techniques for freeze–clamping and for cutting and milling frozen tissue at low temperature for the purpose of two- or three-dimensional metabolic studies *in vivo*, *Anal. Biochem.* **108**:237–248.
43. Ji, S., Chance, B., Nishiki, K., Smith, T., and Rich, T., 1979, Micro-light guide: A new method for measuring tissue fluorescence and reflectance, *Am. J. Physiol.* **236**:C144–C156.
44. Chance, B., Legallais, V., Sorge, J., and Graham, N., 1975, A versatile time-sharing multichannel spectrophotometer, reflectometer, and fluorometer, *Anal. Biochem.* **66**:498–514.
45. Quistorff, B., 1980, Guillotine freeze–clamping of rat brain: Analysis of energy metabolites along the freezing gradient, in: *Cerebral Metabolism and Neuronal Function* (J. V. Passonneau, R. A. Hawkins, W. D. Lust, and F. A. Welsh, eds.), pp.42–52, Williams & Wilkins, Baltimore.
46. Quistorff, B., and Poulsen, H., 1980, Evaluation of a freeze–clamping technique designed for two- and three-dimensional metabolic studies of rat liver *in vivo:* Quenching efficiency and effect of clamping on tissue morphology, *Anal. Biochem.* **108**:249–256.
47. Williamson, J. R., Scholtz, R., Browning, E. T., Thurman, R. G., and Fukami, M. H., 1969, Metabolic effects of ethanol in the perfused liver, *J. Biol. Chem.* **244**(18):5044–5054.
48. Quistorff, B., and Chance, B., 1977, Three-dimensional mapping of metabolic state of rat liver: Effects of high and low alcohol concentrations, *Hoppe-Seyler's Z. Physiol. Chem.* **358**:1261.
49. Häussinger, D., 1983, Hepatocyte heterogeneity in glutamine and ammonia metabolism and the role of an intracellular glutamine cycle during ureogenesis in perfused rat liver, *Eur. J. Biochem.* **133**:269–275.
50. Kashiwagi, T., Ji, S., Lemasters, J. J., and Thurman, R. G., 1981, Rates of alcohol dehydrogenase-dependent ethanol metabolism in periportal and pericentral regions of the perfused rat liver, *Mol. Pharmacol.* **21**:438–443.
51. Ji, S., Lemasters, J. J., and Thurman, R. G., 1980, A non-invasive method to study metabolic events within sublobular regions of hemoglobin-free perfused liver, *FEBS Lett.* **113**(1):37–41.
52. Jöbsis, F. F., and Lamanna, J. C., 1978, Kinetic aspects of intracellular redox reactions, in: *Extrapulmonary Manifestations of Respiratory Disease* (E. Robin, ed.), pp. 63–106, Marcel Dekker, New York.